Pyroclastic Stones as Building Materials in Medieval Romanesque Architecture of Sardinia (Italy): Chemical-Physical Features of Rocks and Associated Alterations

Stefano Columbu, M. Palomba, F. Sitzia, G. Carcangiu & P. Meloni

Taylor & Francis
Taylor & Francis Group

Check for updates

Pyroclastic Stones as Building Materials in Medieval Romanesque Architecture of Sardinia (Italy): Chemical-Physical Features of Rocks and Associated Alterations

Stefano Columbu[a], M. Palomba[b], F. Sitzia[a], G. Carcangiu[b], and P. Meloni[c]

[a]Dipartimento di Scienze Chimiche e Geologiche, University of Cagliari, Cittadella Universitaria di Monserrato, Cagliari, Italy; [b]Istituto di Scienze dell'Atmosfera e del Clima (ISAC) del C.N.R., Sede di Cagliari, C/o Dipartimento di Fisica, Università di Cagliari, Cagliari, Italy; [c]Dipartimento di Ingegneria Meccanica, Chimica e dei Materiali, Università Degli Studi di Cagliari, Cagliari, Italy

ABSTRACT

The paper discusses the chemical-physical-petrographic features and decay processes of *San Nicola* Church (11th–14th century) building materials, one of the most representative Medieval Churches in Sardinia, stylistically attributable to the Romanesque architecture. The monument was built up into two stages and shows a characteristic size uniformity of the ashlars. The masonry is mainly made up of rhyodacitic pyroclastites belonging to the Sardinian Eocene-Miocene magmatic phase (38–15 My). These volcanic rocks were widely used in Medieval architecture for the excellent workability, but its minero-petrographic features greatly favor the decay, due to the action of chemical-physical alteration processes. Although the alteration degree and macroscopic forms of decay vary from zone to zone in the monument, according to the different compositional features of the volcanic stones, weathering and exposure condition, the pyroclastic rocks are generally affected by greater alteration than other igneous lithotypes, due to their petrographic-volcanological characteristics (e.g., low-medium welding grade, medium-high porosity). The results concerning mineralogical and petrographic features, respectively, carried out by the application of X-Ray Powder Diffraction (XRPD), Optical Microscope (OM), and Scanning Electron Microscope (SEM) techniques, both on fresh building rocks and associated alterations, are here presented and discussed. Furthermore, the relationships between fresh pyroclastites and alteration processes affecting these rocks will be discussed.

1. Introduction and aims

The research reports on the results of physical-chemical, mineralogical and petrographic analyses and associated alterations of the original construction materials of the Romanesque *San Nicola* Church (Figures 1 and 2) that dominates the Ottana village (Central Sardinia, Figure 3) from a hill (Figure 2a). It was built up over a pre-existing Church, found during the restoration works made up in 1973–1976. The *Othana Diocese* is documented in 1112 ("*Iohannes episcopus othanensis*"), based in Orotelli in 1116–1139, and moved to Ottana during the period from 1160–1502, when it was integrated to the Churches of Santa Maria di *Castra* and Sant'Antioco di *Bisarcio*.

The Romanesque structure of *San Nicola* Church is defined as *crux commissa*, with oriented apse, barrel-vaulted transept, single-nave hall with a wooden roof. The construction of the masonry took place into two stages: during the former, the apse, the transept, and the Northern side were built up; during the latter stage, the façade and the Southern flank were completed. The

unified character of the structure is evidenced by the medium size uniformity of the ashlars (Coroneo 1993).

Sardinian Medieval Churches (from the 11th–14th century) were built up in a significant and complex historical and geo-political context: at that time, the Island territory was divided into different kingdoms, called *Giudicati* (Serra 1988). The Churches built up in this period are stylistically attributable to the Romanesque architecture.

Romanesque Churches represent one of the best-preserved parts of the Sardinian artistic heritage (Beccaluva et al. 1989, 2005a, 2005b, 2011, Lustrino et al. 2011; Columbu, Gioncada, and Lezzerini 2014b; Columbu et al. 2019b, 2014c, 2018d; Columbu and Verdiani 2014). Many factors played an important role as concerns their conservation in time. Of about 180 churches that still survive, the most were exclusively built up using cut-stones. Moreover, the absence of earthquakes in Sardinia, as well as a lack of important restoration interventions in the centuries (Coroneo 1993; Coroneo and Columbu 2010; Coroneo and Serra

Figure 1. The *San Nicola* Church: (a) main façade; (b) detail on the front door of the Church, which highlight the use of ignimbrite facies of different colors, from red-rose to greyish to blackish; (c) central arch detail under the roof of the Church, with evident loss of cohesion, material detachment from the cornice, corbels, and capitals, and exfoliation in pilaster strips; and (d) details of the mullioned window, which evidence the decohesion, exfoliation, and flaking of the ashlars under the main cornice of the façade.

2004; Delogu 1953), all have contribute to their preservation.

Different rock-types were used in Middle Ages to build up churches, basilicas, and castles in Sardinia (Coroneo 1993). As the use of a particular lithology in the monument building is strongly related to the local availability of materials, the most common used in the construction of Romanic churches, as well as in other ancient times, were magmatic and sedimentary rocks (Columbu et al. 2018b; Columbu and Garau 2017;

Columbu, Garau, and Lugliè 2019c; Columbu et al. 2017a; Verdiani, G., and S. Columbu. 2010), largely spread in the Island; metamorphic rocks, especially marbles, which were used in Roman times in all Mediterranean area along with other materials (Antonelli et al. 2014a, 2014b; Columbu et al. 2014a; Columbu, Antonelli, and Sitzia 2018a; Columbu et al. 2018c; Columbu, Sitzia, and Ennas 2017b; Lezzerini et al. 2016, 2018; Miriello et al. 2015, 2019; Ramacciotti et al. 2018, 2019; Raneri et al. 2018;

Figure 2. The *San Nicola* Church: (a) South-West side overview; (b) South side of the façade overview and Western transept of the Church, where upper and middle parts are covered by whitish patinas; (c) details of the three arches in the front door of the Church, where whitish patinas occur under the horizontal cornice; (d) basal plinth of the main façade, where important processes of exfoliation and flaking occur, causing detachment of flakes up to 2 cm thick; (e) the apse view, with presence of whitish patinas (at the top) and beige/ochre fouling (in the middle and lower parts); and (f) the Western side of the Church, with presence of whitish patinas and organic films (mainly lichens) in the low plinth and in some ashlars.

Columbu, Verdiani and Sitzia 2015b), less commonly outcropping on the Sardinian territory, were seldom used. Metamorphic rocks, as well as basic volcanic rocks (e.g., basalts, phonolites, etc.), were especially used for the ancient production of tools in Nuragic time (Bertorino et al. 2002).

The economic-logistic, as well as the aesthetic and stylistic, choices of the construction materials is generally independent from a preliminary assessment of their compositional features; thus, the action of the decay processes affects the geomaterials in different ways, because each stone has own specific chemical features and physical-mechanical strength (Macciotta et al. 2001). Consequently, the effects of the decay are particularly manifested over the time.

Volcanic rocks are the most commonly used stonework in Sardinia, due to their spread on the territory and excellent workability. But, pyroclastic rocks are
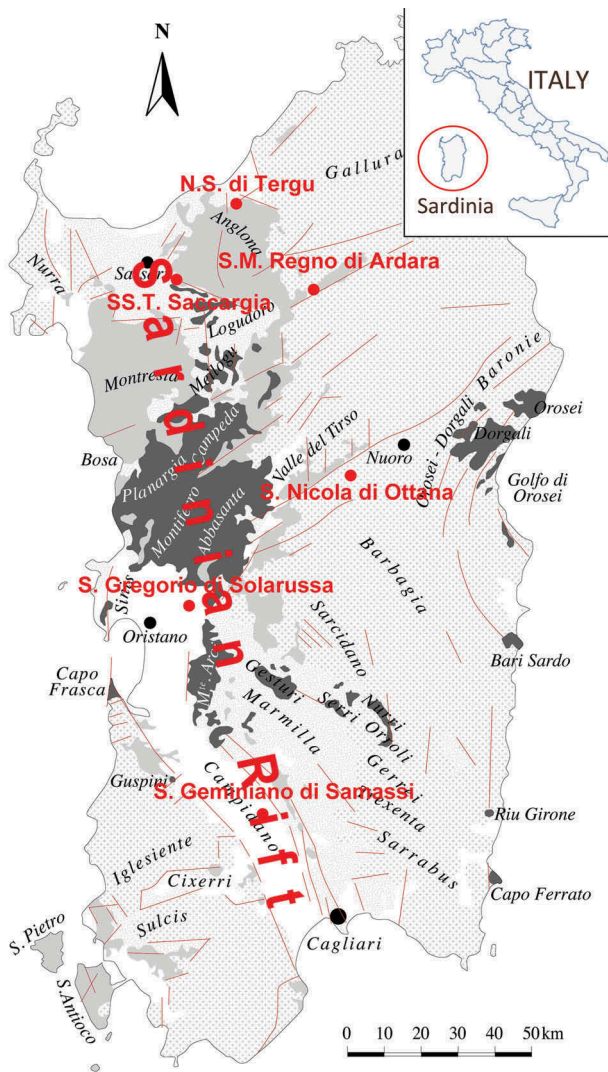
Figure 3. Geological sketch-map of Sardinia, with the localization of the *San Nicola* of Ottana Church and other important Romanesque Churches, built up using volcanic rocks. Legend of patterns and colors referred to lithologies: white = recent alluvial sediments; light grey = Oligocene-Miocene volcanics; dark grey = Pliocene-Pleistocene volcanics; grey dots = Miocene marine sediments; grey crosses = Paleozoic crystalline basement and Mesozoic formations; red continuous and dashed lines = faults.

generally affected by greater alteration than the other igneous lithologies (Columbu et al. 2014a; Columbu, Gioncada, and Lezzerini 2014b; Columbu et al. 2018e; Coroneo and Columbu 2010; Yurtmes and Rowbotham 1999), generally due to their low-medium welding grade (Columbu 2017, 2018; Columbu et al. 2011). The stage and macroscopic forms of decay vary from zone to zone in the stone artifact, according to the intrinsic features of the rock, weathering, and exposure conditions (Figure 2).

The main objective of this paper is the identification of the mechanisms that cause the decay of the pyroclastic stone materials, and their relationships with the compositional features, aimed at the preservation of the monument by means of a proper maintaining and protecting. To achieve this goal, the following studies were performed: (i) mineral-petrographic analyses of the stone materials from *San Nicola* Church; (ii) identification of the secondary mineral phases, formed as consequence of the geochemical transformations caused by weathering alteration on the stone surface; and (iii) determination of the physical-mechanical properties of unaltered ("fresh") and decayed stones, to define the physical decay processes.

2. Materials and methods

2.1. Volcanic rocks and geological setting

San Nicola Church was built up by pyroclastic rocks of the Cenozoic Sardinian volcanism. Pyroclastic occurrences mainly crop out near the Oligocene-Miocene complex NS-trending tectonic structure, known as "*Fossa tettonica sarda*" (Vardabasso and Atzeni 1962) or "*Rift of Sardinia*" (Cherchi and Montadert 1982); see Figure 3. An intense igneous activity is generally associated to the formation of the Rift, and is widely widespread over the entire Island (Advokaat et al. 2014; Cherchi and Montadert 1982; Coulon 1977; Dostal, Coulon, and Dupuy 1982). Volcanic activity is generally related to a deep N-NW-trending subduction zone of the Ionian oceanic lithosphere. Volcanism started in Middle-Late Eocene, below the Paleo-European-Iberian continental margin, and during the Oligocene gave rise to the formation of the rift between Sardinia and Provence (Beccaluva et al. 1989, 2005a, 2011; Burrus 1984; Cherchi et al. 2008).

The pyroclastic rocks used for the *San Nicola* Church construction belong to the early phase of the Cenozoic Sardinian volcanism, and can be related to an orogenic magmatic activity mostly developed during the Late Eocene–Miocene (~ 38–15 My). Major and trace elements, as well as Sr–Nd–Pb–Hf–Os–O isotopes, highlight the complex petrogenetic processes, which include subduction-related metasomatism, hybridization of the mantle and crustal melts, variable degrees of crustal contamination, and fractional crystallization at shallow depths (Lustrino et al. 2013).

The Sardinian orogenic magmatism started in the north of the Island, in the Calabona area (~38 My; Lustrino et al. 2009), as revealed by a small microdiorite outcrop. Other later outcrops occur in Alghero (32.3 ± 1.5 My; Montigny, Edel, and Thuizat 1981); 27.6 ± 1.5 My; Giraud, Bellon, and Turco 1979) and

Osilo (31.2 ± 1.1 My; Montigny, Edel, and Thuizat 1981), as well as in the Cixerri area (Southern Sardinia, 30.2 ± 0.9 My; Beccaluva et al. 1985; 28.3 ± 1 My; Savelli 1975), by andesitic lavas, dacite domes, and rare hypoabyssal outcrops.

Starting from 22 My (Beccaluva et al. 1985; Carminati and Doglioni 2012; Gattaceca et al. 2007; Speranza et al. 2002), a highly explosive fissural activity produced abundant pyroclastic dacitic-rhyolitic products, interlayered by basaltic and andesitic lava flows. The volcanic activity flows occurred in several areas of Sardinia, mainly along the Western graben, N-S trending (Figure 3).

2.2. Sampling and analytical methods

Geological survey on the field and on the *San Nicola* Church, and laboratory investigations on construction materials, were carried out according to the following operative phases: (i) architectural reading and analysis of the structural aspects (plan distribution, building systems, wall textures, etc.); (ii) *in situ* mapping of the macroscopic lithological characteristics of geomaterials, including the decay forms and conservation state; (iii) sampling of materials, in agreement with the representativeness of the lithotypes (according to Recommendations Nor.Ma.L. 3/80 1980); (iv) optical mineral-petrographic, petrophysical, and mechanical studies; (v) mineralogical studies by X-Ray Powder Diffraction (XRPD) analyses; and (vi) mineralogical and morphological studies by Scanning Electron Microscope (SEM) investigations.

A planned thematic sampling of stonework and associated alterations (patinas, efflorescence, crusts, etc.) were carried out both at the surface of rock (outer sample), and on the less altered substrate of rocks (inner sample). Samples were geo-referenced and scheduled. Ground and homogenized samples were studied and analysed by the above-mentioned different analytical techniques.

A total of 23 samples (Table 1) were collected from the shallow parts of the monument masonry, collecting volumes of about 20–25 cm^3, according to the recommendations of the local *Superintendence of Cultural Heritage*, which imposes strict limits on the quantity of sample to be collected. The volumes collected are, however, representative and adequate for the analytical studies. Due to the presence of degradation processes in the stone of the monument (surface decohesion, exfoliation, flaking, efflorescence, etc.), portions of small rock flakes were also sampled for determining, by the XRPD analysis, the possible presence of newly formed phases (e.g., soluble

Table 1. Mineral assemblage of representative selected samples (red-rose rhyodacite = RDR; black rhyodacite = RDB) collected from building materials of *San Nicola* Church, from XRPD data. Legend: Pl = plagioclases, Kf = potassium feldspars, Sm = Smectite-Group minerals (montmorillonite-nontronite series), Il = Mica/Illite Group minerals, Cel and Gla = Celadonite-Glauconite-Group minerals, Gy = gypsum, Ph = polyhalite, Try = tridymite, Cr = cristobalite, GL = glass higher than 80 wt%.

Sample	Material description	Major (> 30 wt%)	Minor (30 > wt% > 5)	Trace (< 5 wt%)
SNO 1	RDR — patinas	Pl, Kf		Cel, Sm
SNO 2	RDR	Pl		
SNO 3	RDR — crust	Pl, Kf		Sm
SNO 4	RDR	Pl, Kf		
SNO 5a	RDR — exfoliation	Pl, Kf	Gy	
SNO 5b	RDR — exfoliation	Pl, Kf	Gy, Try, Cr	
SNO 6	RDR	Pl, Kf		
SNO 7	RDB	Pl, Kf, GL		Sm
SNO 8	RDB	Pl		Sm
SNO 9	RDR — crust	Pl, Kf		Gy
SNO 10	RDR — crust	Pl, Kf, GL	Sm	
SNO 10a	Pumice included in sample SNO 10	Pl, GL		
SNO 11	RDR	Pl, Kf	Sm	
SNO 13a	RDB — white crust	Pl	Ph	
SNO 13b	RDB — grey crust	Pl		Sm
SNO 14	RDB — crust	Pl		Sm
SNO 15	RDB — exfoliation	Pl, Kf, GL		Gy
SNO 16a	RDR — exfoliation	Pl, Kf	Try	Cel, Glc
SNO 16b	RDR — crust	Pl, Kf, GL	Gy	Il
SNO 17	RDR — crust	Pl, GL	Gy, Try	Il, Sm
SNO 18	RDB — crust	Pl, Kf		
SNO 19	RDB — crust	Pl, Kf, GL		
SNO 20	RDB — crust	Pl, Kf, GL		Sm

salts), and to make a comparison between the altered part of the rock and the "healthy" part of the substrate.

Prismatic-like specimens (with an average size of 15•15•15 mm) were made up on laboratory for determining the physical and mechanical properties; covered polished thin sections, about 30 μm thick, were also made up for both the optical microscopy and SEM studies.

Mineral assemblage of rock samples was determined using XRPD analytical technique on samples collected from stone ashlars' surface both in "fresh" and altered samples. Data were collected by a Rigaku Miniflex II apparatus, equipped by a monochromator, using Cuk$_\alpha$ radiation, at 30 kV and 30 mA, filter Ni, from 3–90 °2θ, and measuring step 0.02 °2θ. Mineral identification was carried out by JADE 5.0 software using the JCPDS (Joint Committee on Powder Diffraction) Data Base (2010) for search-match phase. The quantitative analyses of some representative samples were performed using the MAUD (Material Analysis Using Diffraction) analysis program mainly based on the Rietveld method (Lutterotti, Matthies, and Wenk 1999).

Contrariwise, in the summary tables, the mineral phases occurring in solid solution will be expressed using the generic name of the membership Group, not by the specific term of the continuous series.

SEM investigations and photomicrographs were performed on undisturbed rock specimens and on metallized polished thin sections with a Zeiss Evo LS 15, equipped with a LaB6 filament as electron source, for providing information about textural parameters of representative samples (fibrous, lamellar, compact, porous morphologies). Energy Dispersive Spectrometry (EDS), by using the INCA OXFORD apparatus equipped with LaB6 as electron source and a solid-state detector X-Max 50 mm, allowed verifying the qualitative presence of chemical elements of specific interest.

Physical tests to define some main properties (helium- and water-open porosity, solid, real and bulk density, water-imbibition and -saturation coefficients) were carried out according to Buosi et al. (2019) and Columbu et al. (2015a, 2015b).

3. Results

3.1. Petrographic characteristics

The *San Nicola* Church (Figure 1) is made up of ashlars deriving from local pyroclastic rocks, very similar to the ignimbritic facies, belonging to the Late Eocene-Miocene volcanic cycle of Sardinia (Beccaluva et al. 1985; Columbu et al. 2011 ; Columbu, Sitzia, and Verdiani 2015b). A wide variety of colors, from blackish to orange-pink, shades of intermediate tonalities, as well as welding grade, are typical of the ignimbrites outcropping in the adjacent areas.

Although the stone ashlars of *San Nicola* Church (Figures 1 and 2) show different colors, from red-rose (*RDR*) to grey-blackish rhyo-dacites (*RDB*), the mineral and petrographic features are quite similar. Macroscopic observations of physical features revealed that *RDR* show a lower welding than the *RDB* rocks.

Microscopic observations by polarizing microscope show that the pyroclastites of the monument have a porphyritic structure (with porphyritic index of 18–23%), due to the presence of following phenocrystals: opaque (about 2 vol%), clinopyroxene (< 5 vol%), amphiboles (i.e., green hornblende, < 2 vol%), abundant plagioclase (15–20 vol%) and rare quartz (<1 vol %). The glass fraction (up to 85 vol%) represents a fundamental part of the investigated rock-type, more frequently present in the *RDB* facies. Hypohyaline mesostasis, and marked isotropic texture are typical of these rock facies (Figure 4b-d). High

amount of lithics is present. The color index ranges from 5–7.

The round-shaped opaque minerals (about 1 vol% of the total rock), generally magnetite and/or Ti-magnetite, are smaller than 1 mm. Clinopyroxene locally shows partial or complete alteration. Green hornblende and plagioclases show anhedral habitus with size ranging from 0.2–1.5 mm. Somewhere, plagioclases are characterized by intense fracturing and alteration; extinction zones are frequent. Uncommon quartz phenocrystals generally show subhedral habitus.

The glassy groundmass is somewhere devitrified in cryptocrystalline minerals unrecognizable by optical microscope, but determinable by SEM studies. Millimetric lithophysae occur partially or completely filled by secondary K-feldspar, iron-rich phyllosilicates, and other secondary minerals (e.g., celadonite and glauconite, identified by XRPD) giving a greenish color in thin sections under polarizing microscope (Figure 4c-f). Fine-grained and mica-like phyllosilicates also fill the intergranular porosity of the rocks. Phyllosilicates unrecognizable by optical studies, and other newly formed mineral phases, are due to devitrification process. Furthermore, the hypohyaline groundmass includes round-shaped opaque crystals (possibly magnetite, < 1 mm in size), K-feldspars, anhedral microliths of plagioclase (about 0.1 mm in size), clinopyroxene (about 0.1 mm in size), and rare quartz.

Microscopic mineral-petrographic studies allow the classification of the sampled rocks as rhyodacites.

3.2. Analytical data

3.2.1. X-Ray diffraction

XRPD analysis (Table 1) of "fresh" rocks collected form the surface of pyroclastic ashlars shows a mineral assemblage consisting of plagioclases and subordinate K-feldspars, representative of the paragenesis of these rocks. Some samples consist only of plagioclase (Figure 5a). K-feldspar can also occur as major mineral (Figure 5b), but generally in minor amounts than the plagioclase. Due to the particularly abundant volcanic glass fraction in the samples, the particularly high spectra background could mask minor/trace mineral phases.

In the more superficial portions (patinas, crusts, exfoliation, Table 1) of the most altered specimens of the monument, the presence of newly formed mineralogical phases, that do not belong to the original paragenesis of the rock, occurs. These secondary phases derive from both syngenetic and epigenetic alteration processes. The early stages of alteration manifest with the formation of smectite-group minerals (generally montmorillonite or nontronite), mainly due to the
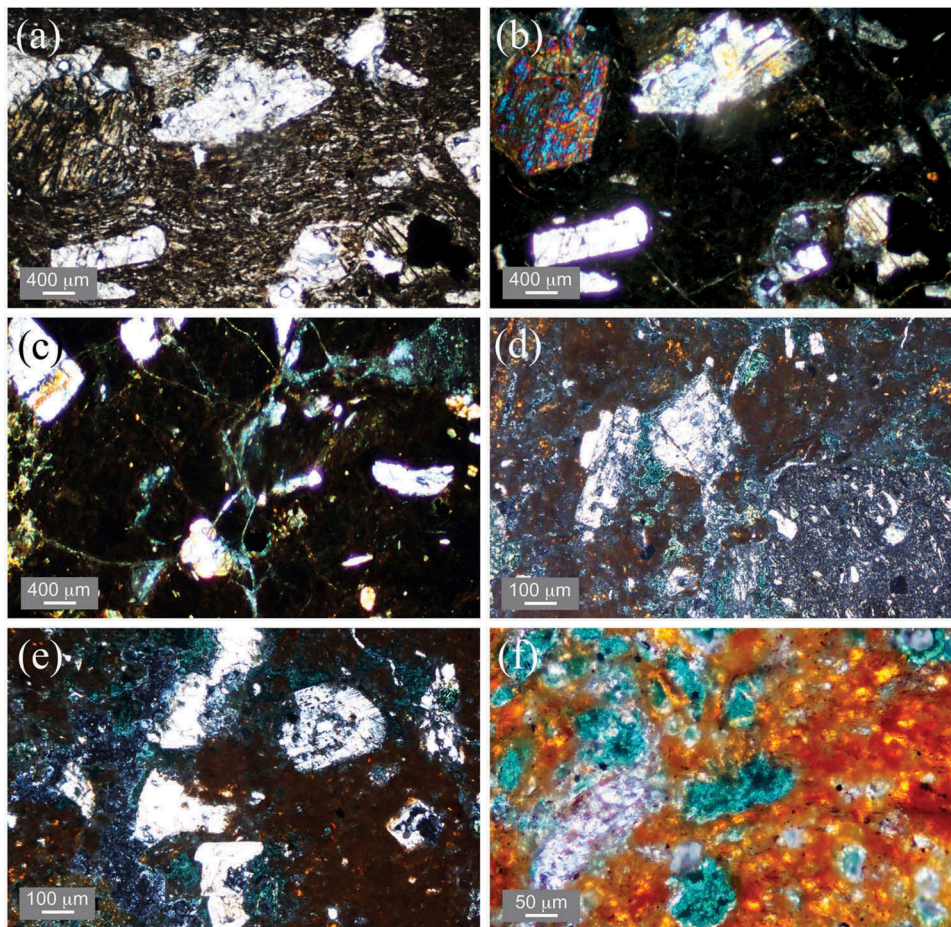
Figure 4. Photomicrographs on thin sections: (a) plane polarized light (PPL): plagioclase and clinopyroxene phenocrystals in glassy matrix, with typical like-fluidal texture and porphyritic structure (porphyritic index from 18–23%); (b) cross polarized light, XPL (same sample of photo a): plagioclase and clinopyroxene phenocrystals in glassy matrix; (c) XPL: plagioclase crystals immersed into glassy groundmass with evident microfractures filled by newly formed greenish phases of celadonite and glauconite; (d, e) XPL: plagioclase crystals immersed into glassy groundmass with secondary greenish phases; and (f) PPL, detail of glassy groundmass, with greenish areas of newly formed celadonite and glauconite.

devitrification process (Figure 6a, Table 1). Smectite-group minerals can occur up to 20 wt% in rich-glass low-grade alteration pyroclastic rock (Figure 6b, Table 1). Illite (< 5 wt%) (Figure 7a,b, Table 1) and gypsum (from 5–15 wt%), as incipient sulphation product of bedding mortars of stone ashlars, can also occur.

In samples containing glass fraction higher than 80 vol%, the presence of K-feldspars can generally be attributable to devitrification of the glassy matrix.

Tridymite and cristobalite are generally detectable in the most altered rocks, as possible devitrification products, but they could also be inherited from the original "fresh" rocks (Figures 7b, 8a, Table 1).

Celadonite $(K(Mg,Fe^{2+})(Fe^{3+},Al)[Si_4O_{10}](OH)_2)$ and/or glauconite $((K,Na)(Fe^{3+},Al,Mg)_2(Si,Al)_4O_{10}(OH)_2)$, phyllosilicates and *end-members* of an isomorphic series, are occasionally detected (Figure 8a, Table 1).

K-Ca-Mg sulphates (Figure 8b, Table 1) are only detected in one sample as minor mineral phases (30 > wt % > 5).

3.2.2. Scanning electron microscope analysis

SEM investigations revealed the presence of an abundant glassy groundmass including the mineral phases like Ca-plagioclases and K-feldspars in major proportion, and subordinately pyroxenes (aegirine and/or augite). Opaque minerals, which composition is consistent with Ti-magnetite and ilmenite phases (Figure 9a) can be also frequently observed widely spread in the glassy matrix. Apatite and biotite can also occur.

Between the newly formed phases due to the alteration, phyllosilicates of the mica/illite group minerals (mainly muscovite, more or less altered into illite) can also occur in minor proportion (Figure 9a,b,e).
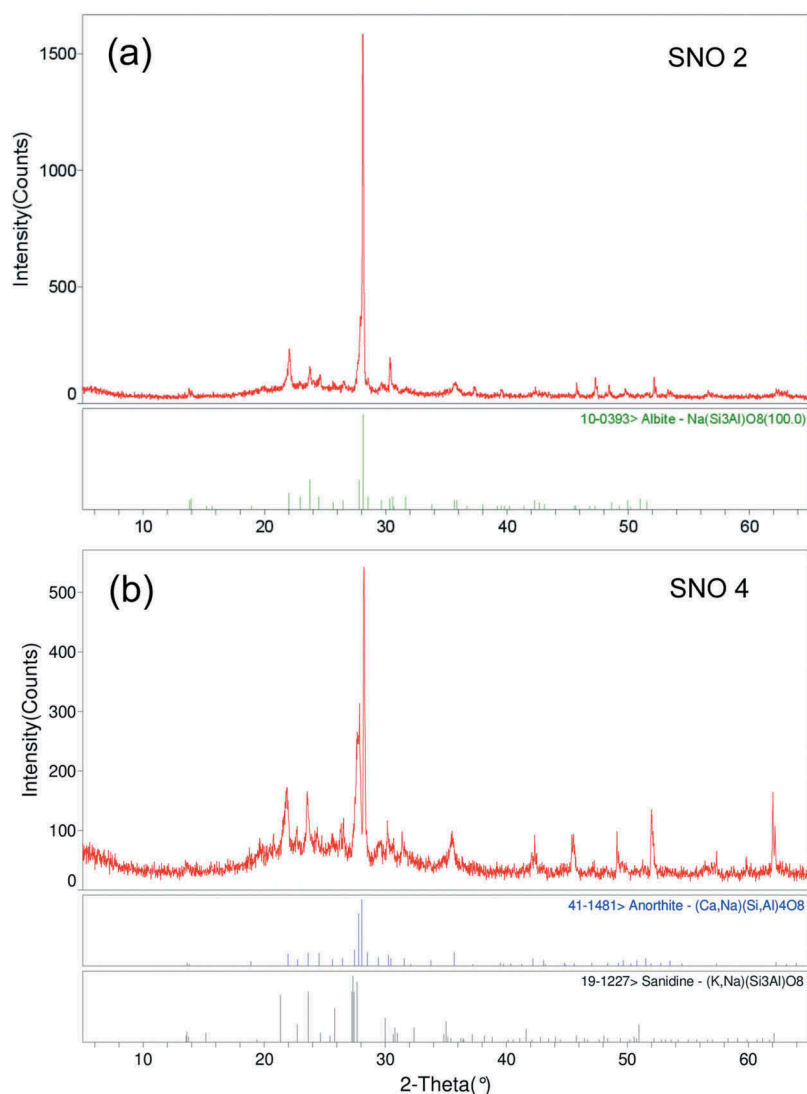
Figure 5. Mineral composition of "fresh" and altered pyroclastic rocks, from XRPD data (for mineral abbreviations, see legend of Table 1): (a) "fresh" sample (SNO 2, glass fraction about 25 vol%); and (b) "fresh" sample (SNO 4, glass fraction about 50 vol%).

SEM observations also show the presence of pumices, partially devitrified in zeolite mineral phases (Figure 9c,d). The zeolite web-like fibers, formed at the expenses of the glass, growth inside the pumices from the rim to the core, and are consistent with the rhyodacitic composition of the volcanic glass (Figure 9c).

Post-genetic secondary fractures (Figure 9e,f), which cross both crystals and matrix, as well as miarolitic micro-cavities, are frequently observed spread into the glassy matrix (Figure 9e,f). Microcavities commonly include a radial-like and/or winding growth of phyllosilicates (Figure 9g,h), generally belonging to the illite-group minerals.

The results of SEM analysis, also by observing the undisturbed samples (i.e., small outer fragments sampled on the stone ashlars), show an intrinsic (mainly syngenetic) diffused microscopic porosity of the rock within the glassy groundmass (<5 μm in size; Figure 9c) and between this latter and the phenocrystals (Figure 9a,b,f). The pores increases (mainly as epigenetic porosity) inside the pumices (with average pore size <15 μm; Figure 9c,d), along the fissuring and micro-fracturing of the glass matrix (about 25–40 μm in size; Figure 9a,b,f), within the miarolitic cavity (ranging from 2–8 μm; Figure 9g,h). A post-genetic porosity (after the laying of stones in the monument) also occurs in the surface of sampled rock fragments, due to the weathering decay.

3.3. Petrophysical tests

Physical tests performed on investigated lithotypes provide fundamental information about the whole
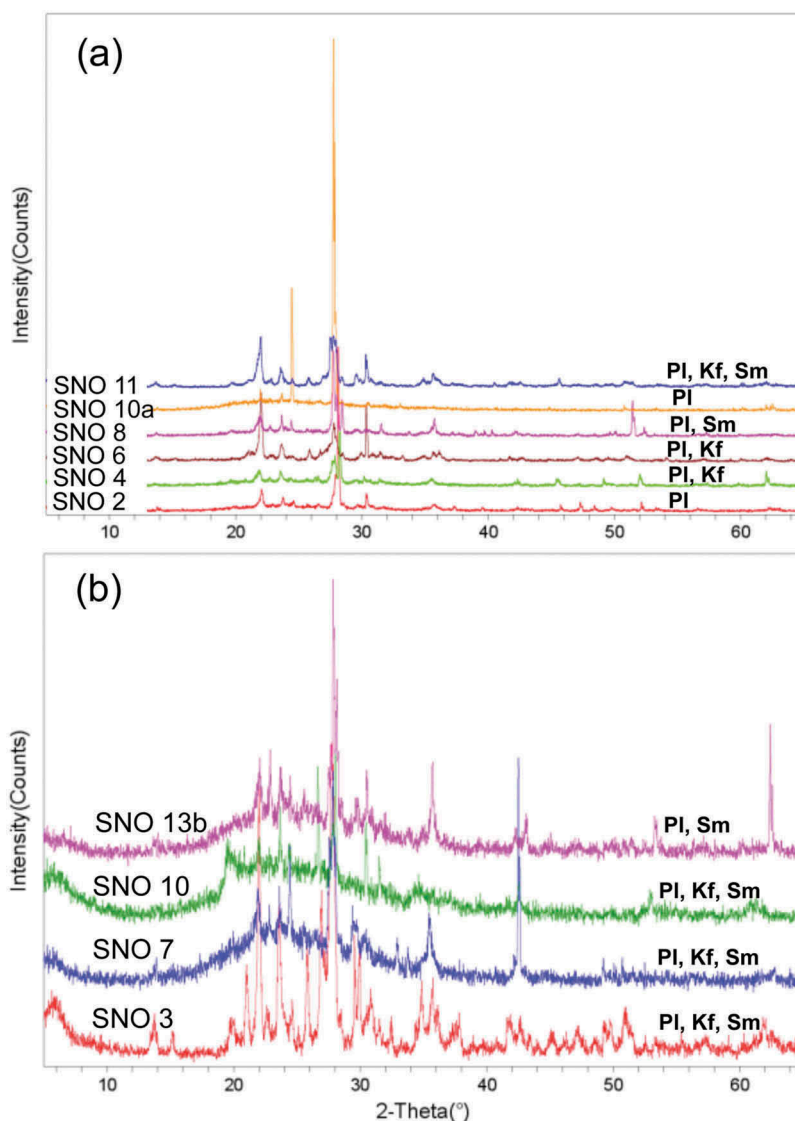
Figure 6. Mineral composition of "fresh" and altered pyroclastic rocks, from XRPD data (for mineral abbreviations, see legend of Table 1): (a) "fresh" samples (SNO 10a, 2, 4, 6) and low-grade alteration samples (SNO 8, 11); and (b) low-grade alteration samples (SNO 13b, 10, 7, 3).

physical-mechanical behavior of the rocks as construction material, and the decay state of the monument samples.

Differences in physical properties were determined between *RDR* and *RDB* pyroclastic lithofacies (Figure 10a,b; Table 2); values relatively variable, even within the same lithotype, were determined. That is closely in correlation with both the different intrinsic physical features of the stone materials (e.g., volcanic welding degree), and especially to the different degree of the sample decay. This latter depends on the different micro-environmental conditions on the monument site. In fact, the chemical-physical alteration processes develop in different ways, substantially in function of the location of samples with respect to the ground level

surrounding the Church, and their exposure to weathering agents.

A different effective syngenetic porosity is in relation with the volcanic emplacement of the pyroclastic rock and/or to a different applied overburden. Water and helium open porosities is rather significant in both *RDR* and *RDB* lithofacies (Table 2), congruent with the average values calculated for the rhyodacitic rocks of other areas from Sardinia (Columbu et al. 2011; Columbu, Gioncada, and Lezzerini 2014b).

RDR is slightly less compact than the *RDB* lithofacies (Table 2; Figure 10a,c), as evidence the average values of the bulk density and total porosity (inversely correlated), 1.82 ± 0.14 g/cm^3 and 32.4 ± 5.7 vol% in the *RDR*, and 2.00 ± 0.13 g/cm^3 and 24.7 ± 4.9 vol%, in the
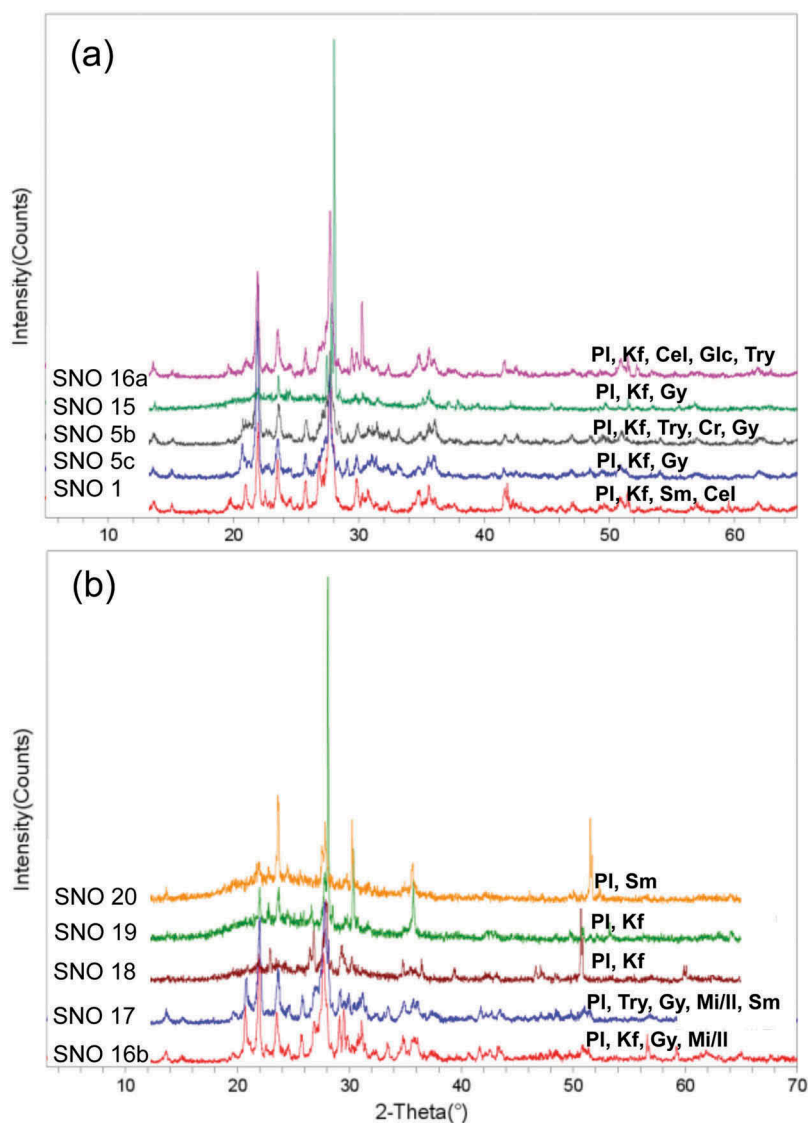
Figure 7. Mineral composition of "fresh" and altered pyroclastic rocks, from XRPD data (for mineral abbreviations, see legend of Table 1): (a) patinas and exfoliations in altered samples (SNO 16a, 15, 5b, 5 c, 1); and (b) crusts in rich-glass altered samples (SNO 20, 19, 18, 17, 16b).

RDB lithofacies. This trend is also highlighted by the water open porosity (ranging from 25.0 ± 4.2 to 19.5 ± 3.3 vol%; Table 2) and especially by the helium open porosity (from 30.7 ± 5.2 to 21.9 ± 4.3 vol%), which represents the effective porosity inter-connected inside the glassy matrix and with the external environment. On the contrary, the closed porosity is generally higher in the *RDB* (on average 2.8 ± 1.6 vol%) than in the *RDR* (1.7 ± 1.2 vol%, Table 2), possibly due to different arrangement of the porous network, i.e., to different pores geometry (with more pore-tortuosity in *RDR*), and pore radius size (smaller in *RDB*). As observed by SEM analyses, a significant part of the total porosity is represented by the secondary one, mainly caused by the alteration processes and chemical-

mineralogical transformation of the glassy matrix, and subordinately by the physical-mechanical decay induced by weathering.

Real density does not show a correlation with bulk density (Figure 10b), while it is closely related to the closed porosity (Figure 10d; Table 2), confirming the above-described differences among porosimetric features.

As regards the hydraulic properties of the rocks, the *RDR* and *RDB* facies show a similar average value of the water saturation index. The saturation index values do not approach the saturation line at 100 vol%, as generally happens for this kind of rocks, with average values of 81.3 and 89.7 vol%, respectively (Table 2; Figure 10c), indicating that the water absorption of
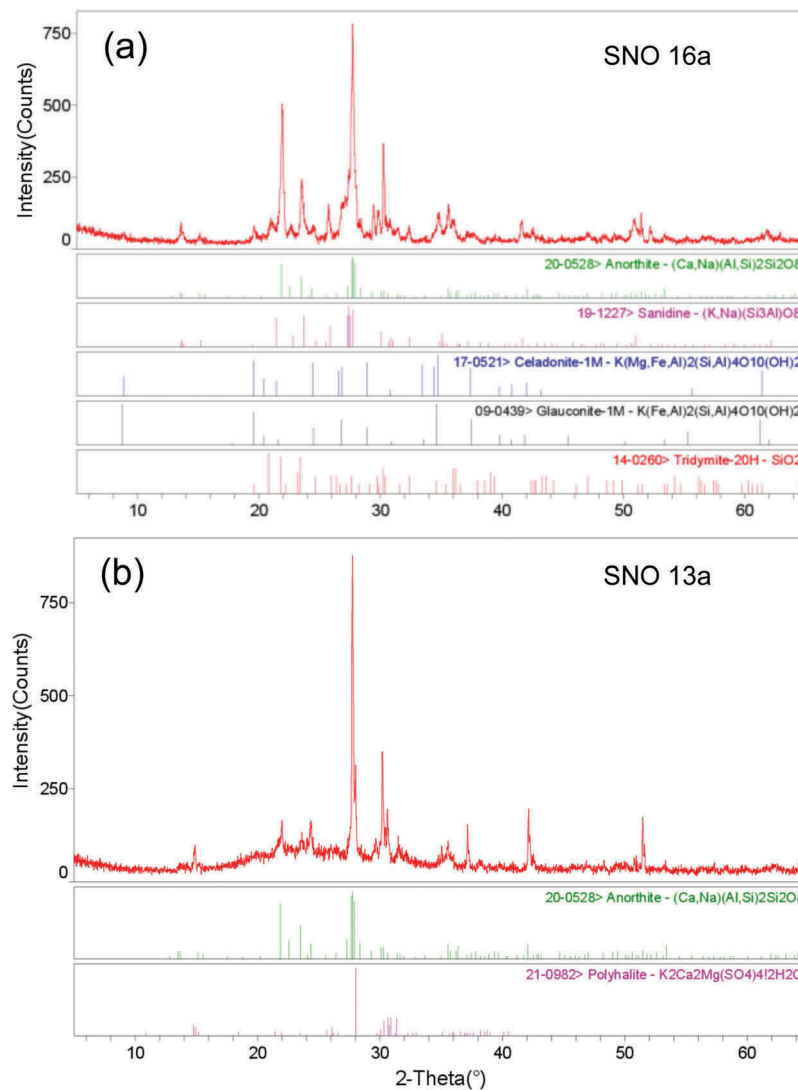
Figure 8. Mineral composition of "fresh" and altered pyroclastic rocks, from XRPD data (for mineral abbreviations, see legend of Table 1): (a) an exfoliation fragment in altered sample (SNO 16a); and (b) a crust fragment in altered sample (SNO 13a).

the sample is rather hindered by the tortuosity of the fine-size porous rock network. In fact, taking into account the presence of hygroscopic newly formed mineral phases (e.g., phyllosilicates, zeolites) in these volcanic samples, the saturation index could be more higher than 100 vol%, as also observed in other similar Sardinian pyroclastic rocks (Columbu et al. 2011) containing hygroscopic solid phases.

Standard deviations show that seven of nine measured parameters (Table 2) are always lower in the *RDB* lithofacies (except for real density and closed porosity parameters; Table 2), as well as the correlation degree (R^2; Figure 10c, 10d), generally greater in the *RDB*. That highlights the lower variability of physical properties in *RDB*, due to its minor syngenetic compositional heterogeneity (i.e., variable glass and crystals amounts), as well as the different alteration grade, weakly higher in the *RDR* lithofacies.

4. Discussion of results

Mineralogical and petrographic studies, performed on stonework making up the structure of *San Nicola* Church, revealed that the pyroclastites are rhyodacitic in composition, with variable occurrences of crystals, lithic fragments, and pumices. The macroscopic differences between *RDR* and *RDB* lithofacies correspond to minor variations in terms of bulk mineral composition and petrographic features (texture, phenocrysts, etc.). Although XRD analysis revealed that high amount of glass (up to 85%) can occur both in *RDB* and *RDR* lithofacies (Table 1, Figure 5d), both detail optical microscopic studies and the lower solid and real densities values evidence that glassy component prevails in the *RDB* facies. Both lithofacies are generally affected by physical decay (decohesion, exfoliation, alveolation,
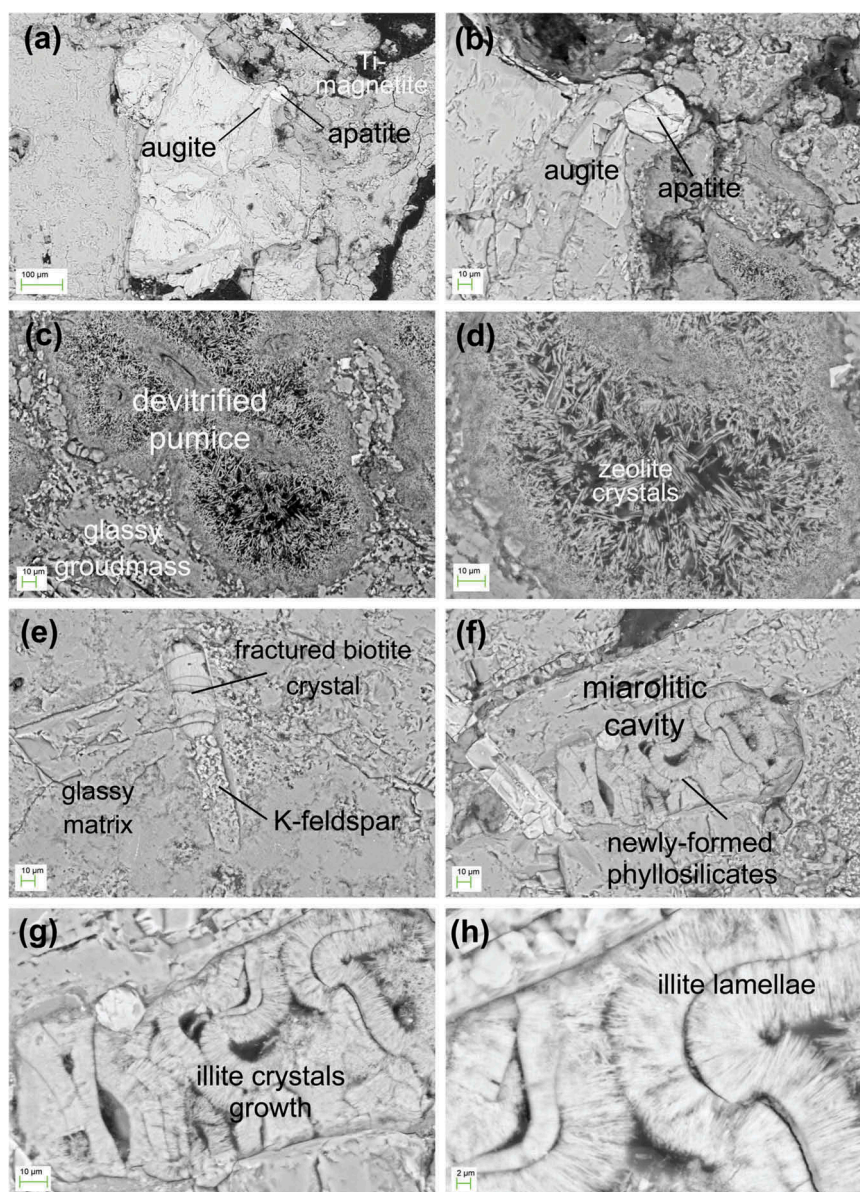
Figure 9. SEM photomicrographs (Secondary Electron images) showing: (a) broken augite crystal inside the glassy groundmass. Ti-magnetite (about 10 microns in size) and ilmenite crystals also occur; (b) augite and apatite crystals (detail of photo (a)); (c) pumice partially devitrified in zeolite; (d) zeolite web-like fibres formed at the expenses of the volcanic glass (detail of photo (c)); (e) biotite crystal and post-genetic fractures, crossing both the mineral and the glass matrix, next to a crystal relic of K-feldspar; (f) miarolitic cavity filled by winding growth of newly formed phyllosilicates; and (g) and (h) packaging of the illite-group mineral lamellae growth inside the cavity (detail of photo (f)).

etc.), while the chemical process post-laying of the stone ashlars in the Church, due to the intrinsic silicatic compositional features of the rock-type and a greater velocity of physical processes, are less evident in the monument. The decay especially affects the external portion of the pyroclastic stones, approaching to the surface exposed to the weathering agents, where the physical process can modify the microstructure of rock, increasing the total porosity of stone. That especially occurs in the *RDR* facies (with values up to 41 vol %), characterized by a higher intrinsic total porosity (on average 32 vol%) with respect to the *RDB* (25 vol %), due to a lower welding degree, as lower solid density (2.67 in *RDR* vs. 2.63 g/cm^3 in *RDB*) and real density (2.63 vs. 2.56 g/cm^3) confirm. The devitrification of glass, due to the syn- and epigenetic alteration processes, can give rise, in some samples, to the formation of silica phases like trydimite and cristobalite.

In the most altered surface portions of the samples collected (crusts, patinas, efflorescence, etc.) newly
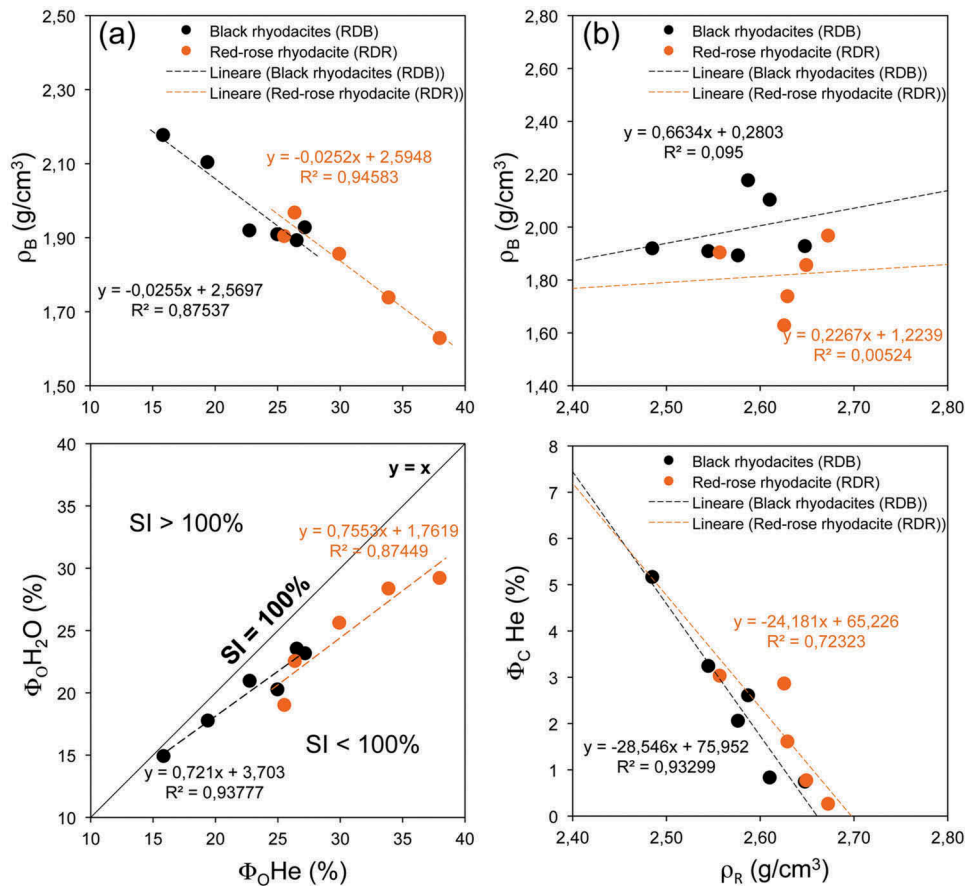
Figure 10. Plot of physical tests: (a) helium open porosity vs. bulk density; (b) real density vs. bulk density; (c) real density vs. closed porosity; (c) helium open porosity vs. water open porosity; and (d) real density vs. helium closed porosity. For legend see the caption of Table 2.

Table 2. Physical data of monument samples (red-rose rhyodacite = RDR; black rhyodacite = RDB) from laboratory tests. Legend: ρ_S = solid density (computing only the solid amorphous (glass) and crystalline phases); ρ_R = real density (computing the solid phases and closed pores to helium); ρ_B = bulk density (computing the solid phases, and total pores); Φ_O He = open helium porosity; Φ_O H_2O = open water porosity; Φ_C He = closed helium porosity; Φ_T = total porosity (i.e., open + closed helium porosities); IC_W = water imbibition coefficient (wt%) after total immersion of specimens; SI = water saturation index (absorbed water vol% related to helium porosity vol%). **Note**: the solid density is determined on the powered-rock specimens, while all other parameters are determined on the undisturbed rock samples.

Sample	Lithology	Specimen type	ρ_S g/cm³	ρ_R g/cm³	ρ_B g/cm³	Φ_OHe %	$\Phi_O H_2O$ %	Φ_CHe %	Φ_T %	IC_W %	SI %
SNO 1	Red-rose rhyodacite	Crust	2,67	2,65	1,86	29,9	25,6	0,8	30,7	13,8	85,7
SNO 6	(RDR)	"fresh"	2,63	2,56	1,90	25,5	19,0	3,0	28,5	10,0	74,6
SNO 9		"fresh"	2,68	2,67	1,97	26,4	22,6	0,3	26,6	11,5	85,6
SNO 16		Flake	2,67	2,63	1,74	33,9	28,4	1,6	35,5	16,3	83,8
SNO 17		Crust	2,70	2,63	1,63	38,0	29,2	2,9	40,8	17,9	77,0
	Average	**Average**	**2,67**	**2,63**	**1,82**	**30,7**	**25,0**	**1,7**	**32,4**	**13,9**	**81,3**
	St. Dev.	**St. Dev.**	**0,02**	**0,04**	**0,14**	**5,2**	**4,2**	**1,2**	**5,7**	**3,3**	**5,2**
SNO 3	Black rhyodacite (RDB)	Crust	2,67	2,65	1,93	27,2	23,2	0,7	27,9	12,0	85,3
SNO 7		"fresh"	2,63	2,61	2,10	19,4	17,8	0,8	20,2	8,4	91,8
SNO 8		Flake	2,63	2,58	1,89	26,5	23,6	2,1	28,6	12,4	88,8
SNO 14		Flake	2,61	2,48	1,92	22,7	21,0	5,2	27,9	10,9	92,2
SNO 18		Crust	2,63	2,54	1,91	25,0	20,3	3,2	28,2	10,6	81,3
SNO 19		"fresh"	2,65	2,59	2,18	15,8	14,9	2,6	18,4	6,9	94,3
	Average	**Average**	**2,63**	**2,56**	**2,00**	**21,9**	**19,5**	**2,8**	**24,7**	**9,9**	**89,7**
	St. Dev.	**St. Dev.**	**0,01**	**0,05**	**0,13**	**4,3**	**3,3**	**1,6**	**4,9**	**2,2**	**5,1**

formed mineral phases occur. XRPD analyses pointed out that primary mineralogy controls the newly formed mineral associations, as well as the intensity of the

alteration. Newly formed minerals occur in both lithofacies as chemical alteration products: the most common species belong to the Clay Group. They are more

or less ubiquitous and occur in different amounts in different samples. Very common are the minerals belonging to the Smectite Group (in particular, the montmorillonite-nontronite series), which mainly form at the expenses of the volcanic glass, fundamental component of these rocks. They occur in variable amounts, ranging from < 5–20 wt%; major contents in smectites mainly occur in samples particularly enriched in the amorphous glass phase. Illite, originating from alteration of the micas, does not exceed 5 wt%.

Other newly formed minerals, like phyllosilicates belonging to the Celadonite-Glauconite Group, sporadically occur in amounts not exceeding 5 wt%.

Also, K-Ca-Mg sulphates, like gypsum and polyhalite, which mainly occur in patinas, exfoliations, and crusts, were occasionally detected in different amounts. Gypsum is the most abundant sulphate phase detected, originating from sulphation phenomena, which favor and allow the recombination of calcium, contained in the feldspars and in volcanic glass, with sulphur carried by the acid rains. The gypsum, in the samples of *San Nicola* Church, occurs from traces to minor occurrence. Polyhalite ($K_2Ca_2 Mg(SO_4)_4 \cdot 2H_2O$), a sulphate salt, was detected as efflorescence in one sample the of *San Nicola* Church, in amounts not exceeding 5 wt%. SEM studies, besides to confirm the presence of primary and newly formed minerals well evidenced by XRPD technique, highlight the occurrence of other primary accessory minerals, undetectable by diffractometry, because of the content in the sample are below the detection limit. Augite, Ti-magnetite, ilmenite, and biotite crystals are quite common species, and generally occur inside the glassy matrix. Among the newly formed minerals, only detectable by SEM studies, Zeolite-Group minerals locally occur in minor proportion. They generally occur as products of devitrification of the pumices and/or web-like fibres formed at the expenses of the volcanic glass. SEM studies also evidence structural and textural aspects of the rocks. The typical anisotropy is highlighted by the fluidal-like texture due to the orientation along a preferential direction of glass shards, crystals, pumices, and lithic fragments. The presence of microstructural discontinuities, and open/closed micropores, also characterizes the study lithofacies. Micro-fractures are generally filled by newly formed mineral species like zeolites.

5. Conclusions

The investigations evidence that the rhyodacitic ignimbrites used as construction geomaterials in the *San Nicola* Church show a chemical-physical decay mainly on the surface of stone ashlars, while overall the monument shows a good durability. On the macroscopic base, the decay is mainly represented by surface decohesion, exfoliation, and flaking processes, these latters generally responsible of the rock breakdown, and subordinately by the presence of efflorescence. The *RDR* and *RDB* lithofacies do not apparently show marked differences in the alteration degree. However, the results of research highlight that the *in situ* decay processes mainly affect the *RDR* lithofacies, due to its different petrophysical features, characterzied by a lower welding degree and then by a greater porosity than *RDB* lithofacies. Thus, water absorption capacity and water open porosity are the main features strongly affecting the durability of the ignimbrites. Open porosity to water, in particular, is the key-element in the channeling of saline solutions through fractures and micro-fractures of the rocks that are, as also the SEM studies evidence, detrimental for the affected materials. The greater open porosity in the *RDR* (ranging from 19–29 vol%) than *RDB* lithofacies (15–24 vol%) affects the physical decay process. For this reason, the *RDR* lithofacies were probably used less than the *RDB* in the construction of the Church. In any case, since both the lithofacies have a relatively high absolute porosity, the presence of circulating water-solutions may cause damages, due to the cyclic crystallization/solubilization of salts. That fact involved destructive effects inside the pore network of rock, with an exponential increase of the effective porosity between the crust/flake and "fresh" portions, calculated up to about 50%. This mechanism favors the stone decay in both *RDR* and *RDB*, in particular, advancing the decohesion and exfoliation processes in the ashlar stone surface. Obviously, physical-mechanical decay is more intense and faster in rocks characterized by intrinsic high porosity (> 25 vol %), due to an easier absorption of liquid phases. Integrated petrographic and analytical studies prove that the chemical-mineralogical alteration state of pyroclastic rocks is mainly due to devitrification degree of glassy matrix of these rocks, which started during syngenetic or immediately post-genetic processes, by geochemical transformations and formations of newly formed phases (i.e., phyllosilicates belonging to smectite, illite, zeolite, celadonite groups, etc.). Furthermore, the alteration of these ignimbritic stones can be subordinately attributed to epigenetic/weathering processes, which cause an increase of the chemical transformations on the stone surface, favoring the formation of clay minerals, frequent albitization of plagioclase, oxidation of mafic phases (e.g., piroxene, amphibole). The presence of gypsum, besides the recombination of calcium of the feldspars and volcanic

glass with sulphur of acid rains, can be also attributed to sulphation process of ancient lime-mortars.

Weathering processes favor and enhance the physical decay of ignimbrite, which frequently masks the chemical decay because on stone surface prevails. Weathering processes especially affect the basal zones of monument, where circulating water solutions concentrate, and in the northward façades, where the moisture in large amount occurs in the wall, and evaporates with difficulty. In these zones of the Church the physical decay affects the rocks by crystallization/solubilization of salts, hydric dilatation of stone matrix, and differential thermal dilatation are the most important decay phenomena, which affect the monument rocks. The most evident macroscopic alteration forms are exfoliation, flaking, fracturing, alveolation, chromatic surface alteration, and presence of fano- and sub-efflorescence.

Chemical-physical alteration processes particularly affect the shallower parts of the ashlars and, although the rocks show a high degree of porosity, the channeling of salt solutions, and consequent cyclic crystallization/solubilization of salt, have so far not compromised the integrity of the rock in depth.

On the whole, the analyses and tests carried out on the masonry structure of *San Nicola* Church provide information about the good durability in time of building materials to the action of alteration phenomena. Despite all of the above, the decay processes are not so important to cause severe damages to the monument structure.

As a demonstration of this, only few and non-invasive restoration interventions can be observed in the *San Nicola* Church, consisting of a limited replacement of stone ashlars, mainly lighter color pyroclastites (light gray-rose to reddish, similar to the *RDR* facies), probably to highlight the intervention performed on the building.

The study of the compositional (chemical-mineralogical and petrographic) and physical characteristics of the pyroclastites, through the comparative study of "fresh" (less altered) samples and more altered ones belonging to superficial portions of rock (crusts, flakes, efflorescence), is certainly useful for understanding the evolution of degradation in construction materials and address the conservative interventions. To avoid the advance of chemical-physical decay of materials, the following two interventions could certainly be useful: (1) perfect efficiency of the Church roof, which must therefore always be well maintained, as it represents the first source of infiltration of rainwater, which by percolating can interact with geomaterials, including also bedding mortars of stone ashlars (usually with a lime base, or in any case not very hydraulic), by leaching, dissolution, and reprecipitation processes of harmful compounds, including gypsum, already locally present; and (2) avoid that various anthropic works carried out around the Church (e.g., flower beds, plants, meadows, etc.) can represent an important source of aqueous solutions infiltration and circulating below the external floor; that can consequently entail the diffusion of salts and compounds equally harmful for the state of conservation of the materials, as they entail a physical-mechanical decay induced by the solubilization/crystallization of soluble salts. In these cases it is recommended to carry out works of regimentation of the meteoric waters that fall around the monument (e.g., by the construction of geopolymer waterproofed floors), for chaneling the aqueous solutions away from the Church.

Disclosure statement

Funding

References

Advokaat, E. L., D. J. J. Van Hinsbergen, M. Maffione, C. G. Langereis, R. L. M. Vissers, A. Cherchi, R. Schroeder, H. Madani, and S. Columbu. 2014. Eocene rotation of Sardinia, and the paleogeography of the Western Mediterranean region. *Earth and Planetary Science Letters* 401:183–95. doi:10.1016/j.epsl.2014.06.012.

Antonelli, F., S. Columbu, M. de Vos Raaijmakers, and M. Andreoli. 2014a. An archaeometric contribution to the study of ancient millstones from the Mulargia area (Sardinia, Italy) through new analytical data on volcanic raw material and archaeological items from Hellenistic and Roman North Africa. *Journal of Archaeological Science* 50 (1):243–61. 0305-4403. doi:10.1016/j.jas.2014.06.016.

Antonelli, F., S. Columbu, M. Lezzerini, and D. Miriello. 2014b. Petrographic characterization and provenance determination of the white marbles used in the Roman sculptures of Forum Sempronii (Fossombrone, Marche, Italy). *Applied Physics A* 115(3):1033–40. 0947-8396. doi:10.1007/s00339-013-7938-2.

Beccaluva, L., G. Bianchini, C. Bonadiman, M. Coltorti, G. Macciotta, F. Siena, and C. Vaccaro. 2005b. Within-plate Cenozoic volcanism and lithospheric mantle

evolution in the Western-central Mediterranean Area. In *Crop project — Deep seismic exploration of the Central Mediterranean and Italy*, ed. I. Finetti, 641–64. Elsevier, Amsterdam. Special Volume.

Beccaluva, L., G. Bianchini, C. Natali, and F. Siena. 2011. Geodynamic control on orogenic and anorogenic magmatic phases in sardinia and southern spain: inferences for the cenozoic evolution of the western mediterranean. *Lithos* 180–181:128–137.

Beccaluva, L., G. Bianchini, M. Coltorti, F. Siena, and M. Verde. 2005a. Cenozoic Tectono- magmatic evolution of the Central-western Mediterranean: Migration of an arc- interarc basin system and variations in the mode of subduction. In *Crop project — Deep seismic exploration of the Central Mediterranean and Italy*, ed. I. Finetti, 623–40. Elsevier, Amsterdam. Special Volume.

Beccaluva, L., L. Civetta, G. Macciotta, and C. A. Ricci. 1985. Geochronology in Sardinia: Results and problems. *Rendering Society* 40:57–72.

Beccaluva, L., P. Brotzu, G. Macciotta, L. Morbidelli, G. Serri, and G. Traversa. 1989. Cainozoic tectono-magmatic evolution and inferred mantle sources in the Sardo-Tyrrenian area. In *The lithosphere in Italy. Advances in earth science research*, ed. A. Boriani., M. Bonafede, G. B. Piccardo, and G. B. Vai, Vol. 80, 229–48. Atti Conv. Acc. Naz. Lincei, Roma.

Bertorino, G., M. Franceschelli, M. Marchi, C. Lugliè, and S. Columbu. 2002. Petrographic characterisation of polished stone axes from Neolithic Sardinia, archaeological implications. *Peer Minerals* 71:87–100. Special Issue: Archaeometry and Cultural Heritage.

Buosi, C., S. Columbu, G. Ennas, P. Pittau, and G. G. Scanu. 2019. Mineralogical, petrographic, and physical investigations on fossiliferous middle Jurassic sandstones from central Sardinia (Italy) to define their alteration and experimental consolidation. *Geoheritage* 11(3):729–49. 1867-2477. doi:10.1007/s12371-018-0326-8.

Burrus, J. 1984. Contribution to a geodynamic synthesis of the Provençal Basin (North-Western Mediterranean). *Marine Geology* 55 (3–4):247–69. doi:10.1016/0025-3227(84)90071-9.

Carminati, E., and C. Doglioni. 2012. Alps vs. Apennines: The paradigm of a tectonically asymmetric Earth. *Earth-Science Reviews* 112 (1–2):67–96. doi:10.1016/j.earscirev.2012.02.004.

Cherchi, A., and L. Montadert. 1982. Oligo-Miocene rift of Sardinia and the early history of the western Mediterranean basin. *Nature* 298 (5876):736–39. doi:10.1038/298736a0.

Cherchi, A., N. Mancin, L. Montadert, M. Murru, M. T. Putzu, F. Schiavinotto, and V. Verrubbi. 2008. The stratigraphic response to the Oligo-Miocene extension in the western Mediterranean from observations on the Sardinia graben system (Italy). *Bulletin de la Societe Geologique de France* 179 (3):267–87. doi:10.2113/gssgfbull.179.3.267.

Columbu, S., M. Marchi, R. Martorelli, M. Palomba, F. Pinna, F. Sitzia, L. Tanzini, and A. Virdis. 2014c. Romanesque and Territory. The construction materials of Sardinian Medieval Churches: New approaches to the valorisation, conservation and restoration. *Conference on Cultural Heritage and New Technologies, CHNT 19*, Nov 3-5 2014 Wien, Session: Urban archeology and Processing - Rubble, Ruins and Reading, Specific Approaches in Analysis, Trying to Let the Remains Telling the Story: 23-24. http://www.chnt.at/wp-content/uploads/WS19_Abstractband.pdf

Columbu, S. 2017. Provenance and alteration of pyroclastic rocks from the Romanesque Churches of Logudoro (north Sardinia, Italy) using a petrographic and geochemical statistical approach. *Applied Physics A* 123(3):165. 0947-8396. doi:10.1007/s00339-017-0790-z.

Columbu, S. 2018. Petrographic and geochemical investigations on the volcanic rocks used in the Punic-Roman archaeological site of Nora (Sardinia, Italy). *Environmental Earth Sciences* 77(16):577. 1866-6299. doi:10.1007/s12665-018-7744-4.

Columbu, S., A. Gioncada, and M. Lezzerini. 2014b. Hydric dilatation of ignimbritic stones used in the churchof Santa Maria di Otti(Oschiri, northern Sardinia, Italy). *Italian Journal of Geosciences* 133(1):149–60. 20381719. doi:10.3301/IJG.2013.20.

Columbu, S., A. Gioncada, M. Lezzerini, and F. Sitzia. 2019b. Mineralogical-chemical alteration and origin of ignimbritic stones used in the old Cathedral of Nostra Signora di Castro (Sardinia, Italy). *Studies in Conservation* 0039-3630, doi: 10.1080/00393630.2018.1565016, WOS:000463289900001 64(7):397–422. . doi:.

Columbu, S., and A. M. Garau. 2017. Mineralogical, petrographic and chemical analysis of geomaterials used in the mortars of Roman Nora theatre (south Sardinia, Italy). *Italian Journal of Geosciences* 136(2):238–62. 2038-1727. doi:10.3301/IJG.2017.05.

Columbu, S., A. M. Garau, and C. Lugliè. 2019c. Geochemical characterisation of pozzolanic obsidian glasses used in the ancient mortars of Nora Roman theatre (Sardinia, Italy): Provenance of raw materials and historical–archaeological implications. *Archaeological and Anthropological Sciences* 11(5):2121–50. 18669557. doi:10.1007/s12520-018-0658-y.

Columbu, S., A. M. Garau, G. Macciotta, M. Marchi, C. Marini, D. Carboni, S. Ginesu, and G. Corazza. 2011. *Manuale sui materiali lapidei vulcanici della Sardegna centrale e dei loro principali impieghi nel costruito*, 302. Ghilarza (OR): Iskra Edizioni.

Columbu, S., C. Lisci, F. Sitzia, and G. Buccellato. 2017a. Physical–mechanical consolidation and protection of Miocenic limestone used on Mediterranean historical monuments: The case study of Pietra Cantone (southern Sardinia, Italy). *Environmental Earth Sciences* 76(4):148. 1866-6299. doi:10.1007/s12665-017-6455-6.

Columbu, S., C. Lisci, F. Sitzia, G. Lorenzetti, M. Lezzerini, S. Pagnotta, S. Raneri, S. Legnaioli, V. Palleschi, G. Gallello, et al. 2018c. Mineralogical, petrographic and physical-mechanical study of Roman construction materials from the Maritime Theatre of Hadrian's Villa (Rome, Italy). *Measurement* 127:264–76. 0263-2241. doi:10.1016/j.measurement.2018.05.103.

Columbu, S., F. Antonelli, and F. Sitzia. 2018a. Origin of Roman worked stones from St. Saturno Christian Basilica (South Sardinia, Italy). *Mediterranean Archaeology & Archaeometry* 18(5):17–36. 1108-9628. doi:10.5281/zenodo.1256047.

Columbu, S., F. Antonelli, M. Lezzerini, D. Miriello, B. Adembri, and A. Blanco. 2014a. Provenance of marbles

used in the Heliocaminus Baths of Hadrian's Villa (Tivoli, Italy). *Journal of Archaeological Science* 49(1):332–42. 0305-4403. doi:10.1016/j.jas.2014.05.026.

Columbu, S., F. Sitzia, and G. Ennas. 2017b. The ancient pozzolanic mortars and concretes of Heliocaminus baths in Hadrian's Villa (Tivoli, Italy). *Archaeological And Anthropological Sciences* 9(4):523–53. 1866-9565. doi:10.1007/s12520-016-0385-1.

Columbu, S., F. Sitzia, and G. Verdiani. 2015b. Contribution of petrophysical analysis and 3D digital survey in the archaeometric investigations of the Emperor Hadrian's Baths (Tivoli, Italy). *Rendiconti Lincei* 26(4):455–74. 20374631. doi:10.1007/s12210-015-0469-3.

Columbu, S., G. Cruciani, D. Fancello, M. Franceschelli, and G. Musumeci. 2015a. Petrophysical properties of a granite-protomylonite-ultramylonite sequence: Insight from the Monte Grighini shear zone, central Sardinia, Italy. *European Journal of Mineralogy* 27(4):471–86. 0935-1221. doi:10.1127/ejm/2015/0027-2447.

Columbu, S., G. Piras, F. Sitzia, S. Pagnotta, S. Raneri, S. Legnaioli, V. Palleschi, M. Lezzerini, and M. Giamello. 2018e. Petrographic and mineralogical charecterization of volcanic rocks and surface-depositions on Romanesque monuments. *Mediterranean Archaeology & Archaeometry* 18 (5):37–64. 1108-9628. doi:10.5281/zenodo.1256051.

Columbu, S., and G. Verdiani. 2014. Digital survey and material analysis strategies for documenting, monitoring and study the Romanesque Churches in Sardinia, Italy. *Lecture Notes in Computer Science* 8740(2014):446–53. 03029743. doi:10.1007/978-3-319-13695-0.

Columbu, S., M. Palomba, F. Sitzia, and M. R. Murgia. 2018d. Geochemical, mineral-petrographic and physical-mechanical characterisation of stones and mortars from the Romanesque Saccargia Basilica (Sardinia, Italy) to define their origin and alteration. *Italian Journal of Geosciences* 137(3):369–95. 2038-1719. doi:10.3301/IJG.2018.04.

Columbu, S., S. Carboni, S. Pagnotta, M. Lezzerini, S. Raneri, S. Legnaioli, V. Palleschi, and A. Usai. 2018b. Laser-induced breakdown spectroscopy analysis of the limestone nuragic statues from Mont'e Prama site (Sardinia, Italy). *Spectrochimica Acta, Part B: Atomic Spectroscopy* 149 (2018):62–70. 0584-8547. doi:10.1016/j.sab.2018.07.011.

Coroneo, R. 1993. *Architettura romanica dalla metà del Mille al primo '300, Nuoro, Ilisso*. ISBN 88-85098-24-X

Coroneo, R., and R. Serra. 2004. *Sardegna preromanica e romanica*. Milano: Jaca Book.

Coroneo, R., and S. Columbu. 2010. Sant'Antioco di Bisarcio (Ozieri): La cattedrale romanica e i materiali costruttivi. *Archeoarte* 1:145–73.

Coulon, C. 1977. Le volcanism calco-alcalin cenozoique de Sardaigne, Italie. Unpublished master's thesis., Univesité St. Jerome, Marseille.

Delogu, R. 1953. *L'Architettura del Medioevo in Sardegna. Libreria dello Stato, Roma (ristampa anastatica, Sassari, 1988)*.

Dostal, J., C. Coulon, and C. Dupuy. 1982. Cainozoic andesitic rock of Sardinia (Italy). In *Andesites: Orogenic andesites and related rocks*, ed. R. S. Thorpe, 353–70. Chichester: J. Wiley & Sons.

Gattaceca, J., A. Deino, R. Rizzo, D. S. Jones, B. Henry, B. Beaudoin, and F. Vadeboin. 2007. Miocene rotation of Sardinia: New paleomagnetic and geochronological constraints and geodynamic implications. *Earth and Planetary Science Letters* 258:359–77.

Giraud, J., H. Bellon, and G. Turco. 1979. L'intrusion microdioritique tertiaire d'Alghero (Sardaigne). Age K/Ar et relation avec le magmatism calco-alcalin sarde. Analogies aves les esterellites de l'Esterel (Var). C. R. *Comptes rendus de l'Académie des Sciences* 288:9–12. Paris.

International Centre for Diffraction Data. 2010. *Powder diffraction file JCPDS, inorganic phases*. Newtown Square, Pennsylvania (U.S.A.).

Lezzerini, M., F. Antonelli, S. Columbu, R. Gadducci, A. Marradi, D. Miriello, L. Parodi, L. Secchiari, and A. Lazzeri. 2016. Cultural heritage documentation and conservation: Three-dimensional (3D) laser scanning and geographical information system (GIS) techniques for thematic mapping of facade stonework of St. Nicholas Church (Pisa, Italy). *International Journal of Architectural Heritage* 10(1):9–19. 1558-3058. doi:10.1080/15583058.2014.924605.

Lezzerini, M., S. Raneri, S. Pagnotta, S. Columbu, and G. Gallello. 2018. Archaeometric study of mortars from the Pisa's Cathedral Square (Italy). *Measurement* 126:322–31. 0263-2241. doi:10.1016/j.measurement.2018.05.057.

Lustrino, M., L. Fedele, L. Melluso, V. Morra, F. Ronga, J. Geldmacher, D. Duggen, S. Agostini, C. Cucciniello, L. Franciosi, et al. 2013. Origin and evolution of Cenozoic magmatism of Sardinia (Italy). A combined isotopic (Sr–Nd–Pb–O–Hf–Os) and petrological view. *Lithos* 180–181:138–58.

Lustrino, M., S. Duggen, and C.L. Rosenberg. 2011. The central-western mediterranean: anomalous igneous activity in an anomalous collisional tectonic setting. *Earth-science Reviews* 104 (1-3 doi:10.1016/j.earscirev.2010.08.002):1-40. 1-3 doi: 10.1016/j.earscirev.2010.08.002.

Lustrino, M., V. Morra, L. Fedele, and L. Franciosi. 2009. Beginning of the Apennine subduction system in central western Mediterranean: Constraints from Cenozoic "orogenic" magmatic activity of Sardinia, Italy. *Tectonics* 28:TC5016.

Lutterotti, L., S. Matthies, and H. R. Wenk. 1999. MAUD (Material analysis using diffraction): A user friendly Java program for rietveld texture analysis and more. In: *Proceeding of the Twelfth International Conference on Textures of Materials (ICOTOM-12)*, Jerzy A. Szpunar Ed., McGill University, Montreal, Canada, August 9 - 13, 1999, Vol. 1

Macciotta, G., G. Bertorino, A. Caredda, S. Columbu, R. Coroneo, M. Franceschelli, M. Marchi, and S. Rescic. 2001. The S.Antioco of Bisarcio Basilica (NE Sardinia, Italy): Water-rock interaction in ignimbrite monument decay. *Water-Rock Interaction (WRI-10)*, Villasimius (Italy), June 10-15. A.A. Balkema Publ.

Miriello, D., F. Antonelli, A. Bloise, M. Ceci, S. Columbu, R. D. Luca, M. Lezzerini, A. Pecci, B. S. Mollo, and P. Brocato. 2019. Archaeometric approach for studying architectural earthenwares from the archaeological site of St. Omobono (Rome-italy). *Minerals* 9(5):266. 2075163X. doi:10.3390/min9050266.

Miriello, D., F. Antonelli, C. Apollaro, A. Bloise, N. Bruno, M. Catalano, S. Columbu, G. M. Crisci, R. De Luca, M. Lezzerini, et al. 2015. A petro-chemical study of ancient mortars from the archaeological site of Kyme (Turkey). . *Periodico di Mineralogia* 84(3A):497–517. 03698963. doi:10.2451/2015PM0028.

Montigny, R., J. B. Edel, and R. Thuizat. 1981. Oligo-miocene rotation of sardinia: K-ar ages and paleomagnetic data of tertiary volcanics. *Earth and Planetary Science Letters* 54:261–71.

Ramacciotti, M., S. Rubio, G. Gallello, M. Lezzerini, S. Columbu, E. Hernandez, A. Morales-Rubio, A. Pastor, and M. De La Guardia. 2018. Chronological classification of ancient mortars employing spectroscopy and spectrometry techniques: Sagunto (Valencia, Spain) Case. *Journal of Spectroscopy* 2018 (9736547):1–10. 2314-4920. doi:10.1155/2018/9736547.

Ramacciotti, M., S. Rubio, G. Gallello, M. Lezzerini, S. Raneri, E. Hernandez, M. Calvo, S. Columbu, A. Morales, A. Pastor, et al. 2019. "Chemical and mineralogical analyses on stones from Sagunto Castle (Spain)." *Journal of Archaeological Science: Reports*. 24931–38. 2352409X. doi:10.1016/j.jasrep.2019.03.017.

Raneri, S., S. Pagnotta, M. Lezzerini, S. Legnaioli, V. Palleschi, S. Columbu, N. F. Neri, and P. Mazzoleni. 2018. Examining the reactivity of volcanic ash in ancient mortars by using a micro-chemical approach. *Mediterranean Archaeology & Archaeometry* 18 (5):147–57. 2241-8121. doi:10.5281/zenodo.1285897.

Savelli, C. 1975. Datazioni preliminari col metodo K-Ar di vulcaniti della Sardegna sud-occidentale. *Rendering Society* 31:191–98.

Serra, R. 1988. *Sardegna Romanica*. Jaca Book, Milano. ISBN 88-16-60096-9.

Speranza, F., I. M. Villa, L. Sagnotti, F. Florindo, D. Cosentino, P. Cipollari, and M. Mattei. 2002. Age of the Corsica-Sardinia rotation and Liguro-Provençal Basin spreading: New paleomagnetic and Ar/Ar evidence. *Tectonophysics* 347 (4):231–51.

UNI Nor.Ma.L. Recommendations 3/80. 1980. *Stone materials: Sampling*. Cultural Heritage Technical Commission, Roma (Reprint 1988).

Vardabasso, S., and A. Atzeni. 1962. Il bacino Oligocenico di Oschiri- Berchidda nella Sardegna nord-occidentale. *Memorial Society of Geoscience* 3:717.

Verdiani, G., and S. Columbu. 2010. E.Stone, an archive for the Sardinia monumental witnesses. *Lecture Notes in Computer Science* 6436:356–72. 03029743, ISBN: 3642168728;978-364216872-7. doi:10.1007/978-3-642-16873-4_27.

Yurtmen, S., and G. Rowbotham. 1999. A scanning electron microscope study of post-depositional changes in the northeast niğde ignimbrites, south central anatolia, turkey, South Central Anatolia, Turke. *Mineralogical Magazine* 63 (1):131–41. doi:10.1180/002646199548259